Available online at www.sciencedirect.com
SCIENCE DIRECT
Biomaterials 27 (2006) 4192–4203
Biomaterials
www.elsevier.com/locate/biomaterials

Early bone apposition in vivo on plasma-sprayed and electrochemically deposited hydroxyapatite coatings on titanium alloy

Hao Wang[a,*], Noam Eliaz[b], Zhou Xiang[c,d], Hu-Ping Hsu[c,d], Myron Spector[c,d], Linn W. Hobbs[a]

[a]*Department of Materials Science and Engineering, Massachusetts Institute of Technology, 77 Massachusetts Ave., Cambridge, MA 02139, USA*
[b]*Department of Solid Mechanics, Materials and Systems, Tel-Aviv University, Ramat-Aviv, Tel-Aviv 69978, Israel*
[c]*Tissue Engineering, VA Boston Healthcare System, Boston Campus, 150 S. Huntington Ave., Boston, MA 02130, USA*
[d]*Department of Orthopaedic Surgery, Brigham and Women's Hospital, Harvard Medical School, 75 Francis Street, Boston, MA 02115, USA*

Received 23 January 2006; accepted 21 March 2006

Abstract

Three different implants, bare Ti–6Al–4V alloy, Ti–6Al–4V alloy coated with plasma-sprayed hydroxyapatite (PSHA), and Ti–6Al–4V alloy coated with electrochemically deposited hydroxyapatite (EDHA), were implanted into canine trabecular bone for 6 h, 7, and 14 days, respectively. Environmental scanning electron microscopy study showed that PSHA coatings had higher bone apposition ratios than those exhibited by bare Ti–6Al–4V and EDHA coatings after 7 days; however, at 14 days after implantation, EDHA and PSHA coatings exhibited similar bone apposition ratios, much higher than that for bare Ti–6Al–4V. The ultrastructure of the bone/implant interface observed by transmission electron microscope showed that the earliest mineralization (6 h—7 days) was in the form of nano-ribbon cluster mineral deposits with a Ca/P atomic ratio lower than that of hydroxyapatite. Later-stage mineralization (7–14 days) resulted in bone-like tissue with the characteristic templating of self-assembled collagen fibrils by HA platelets. Though adhesion of EDHA coatings to Ti–6Al–4V substrate proved problematical and clearly needs to be addressed through appropriate manipulation of electrodepositon parameters, the finely textured microstructure of EDHA coatings appears to provide significant advantage for the integration of mineralized bone tissue into the coatings.

Keywords: Bone; Hydroxyapatite coatings; Plasma spraying; Titanium alloy; TEM

1. Introduction

Since their introduction in the 1980s, hydroxyapatite (HA) coatings on orthopedic implants have gained wide acceptance in orthopedic surgery [1]. It has been repeatedly demonstrated clinically that HA coatings have osteoconductive properties, and that the fixation of HA-coated implants is better than for uncoated implants following optimal surgical conditions [2]. Laboratory research also supports the conclusion that the early bone growth and apposition are accelerated by implants coated with HA [3].

Plasma-spraying is still the most popular technology commercially used for depositing HA coatings onto titanium-base and other metal-base implants. However, plasma spraying is a high-temperature and line-of-sight process. Potential problems with this technology include exposure of substrates to intense heat, residual thermal stresses in coatings, and the inability to coat complex shapes with internal cavities [4]. Many other techniques have been explored to address these problems [5], including ion-beam deposition [6], chemical deposition [4], metallo-organic chemical vapor deposition [7], derivation from sol–gels [8], pulsed laser deposition [9], and electrophoresis [10].

Electrochemical deposition is one of the most promising new processes [11,12]. Compared to plasma spraying, the advantages of electrochemical deposition include good control of composition and structure of the coatings, relatively low processing temperatures that enable

*Corresponding author. Tel.: +1 617 9192058; fax: +1 617 7300122.
E-mail address: hao.wang@tch.harvard.edu (H. Wang).

0142-9612/$ - see front matter © 2006 Elsevier Ltd. All rights reserved.
doi:10.1016/j.biomaterials.2006.03.034

formation of highly crystalline deposits with low residual stresses, and the ability to deposit on non-line-of-site, porous or complex surfaces. The structure of the coating can be controlled by changing the composition, pH and temperature of the electrolyte, as well as the applied potential or current density. Various calcium phosphate coatings, including carbonated apatite [12], brushite [13], octacalcium phosphate [14,15], and HA [16,17], have been successfully applied to titanium-base and other alloys by electrochemical deposition.

The earliest stages of mineralization (3 h to 14 days) of new bone forming on plasma-sprayed HA (PSHA) coatings have extensively been studied at MIT by transmission electron microscopy (TEM) [18]. These studies showed that new bone formation on implants was accelerated in the presence of PSHA coatings, the rate of earliest-stage bone formation being influenced by the solubilities of the PSHA coatings. Coatings with higher crystallinity, which exhibited lower solubility in vitro and would be expected to have lower solubility in vivo, exhibited delayed formation of new bone compared to less crystalline coatings with higher solubility. Electrochemically deposited HA (EDHA) coatings exhibit deposition morphologies and crystallinities substantially distinct from those of PSHA. Therefore, the study of early bone formation on EDHA coatings can provide an additional perspective from which to understand the underlying mechanism of new bone formation, as well an assessment of the relative osteoconductivity of EDHA coatings.

In this study, bare Ti–6Al–4V alloy (nominal composition in wt% alloy additions), Ti–6Al–4V coated with PSHA, and Ti–6Al–4V coated with EDHA were implanted into canine trabecular bone for 6 h, 7 and 14 days, respectively, in order to study the initial bone formation on these implant materials. The new bone apposition ratios at different time points were evaluated using environmental scanning electron microscopy (ESEM). The ultrastructures developing at the interface between host bone and HA coatings were studied by TEM.

2. Materials and methods

2.1. Materials

A Ti–6Al–4V ELI grade (ASTM F136-92) rod, 4.76 mm in diameter and 1.83 m long, was purchased from Titanium Industries, Inc. (Parsippany, NJ). This rod was machined into 10.0 mm-long sample rods. Thirty rods were plasma sprayed with HA by Bio-Coat, Inc. (Southfield, MI), in their entirety except for 2 mm at one end which was left uncoated. Thirty rods were electrochemically deposited with HA entirely. Thirty rods were left uncoated, presenting the as-received surface. All 90 rods were sealed in sterilization bags separately, sterilized by ethylene oxide for 2 h, and then left to aerate in laboratory air for at least 2 days before implantation.

Prior to electrodeposition, the exposed alloy surfaces were mechanically ground on 1000-grit SiC paper, followed by 30 min ball milling with 1 μm alumina powder. The alloy rods were then cleaned ultrasonically in acetone. Electrodeposition was carried out in a standard three-electrode cell in which a platinum foil was used as the auxiliary (counter) electrode and a saturated calomel electrode (SCE) as the reference electrode. The electrolyte was prepared by dissolving 0.61 mM $Ca(NO_3)_2$ and 0.36 mM $NH_4H_2PO_4$, both AR-grade from Merck (Darmstadt, Germany), in Millipore water (Milli-DI^{TM}, resistivity $>1\,M\Omega\,cm$; Millipore Corporation, Billerica, MA). The acidity was measured using an InoLab pH/Oxi Level 3 meter (WTW Gmbh, Weilheim, Germany) and adjusted to pH 6.0, so that the electrolyte was saturated with calcium and phosphate ions. During the electrodeposition process, CO_2-free nitrogen gas (99.999% purity) was continuously purged into the electrolyte to minimize the risk of contamination of the deposits with carbonates. In addition, continuous stirring was carried out using a magnetic bar. A Lauda Gmbh (Lauda-Königshofen, Germany) Ecoline model E-220 T thermostatic bath was used to maintain a constant temperature of $85\pm0.1\,^{\circ}C$. An EG&G/PAR (Princeton, NJ) model 263A potentiostat/galvanostat operating in potentiostatic mode was employed to maintain the cathode potential at -1.4 V vs. SCE for 2 h.

The near-surface phase composition of the different implant sample types was studied by powder X-ray diffractometry (Rigaku model RU-200 diffractometer with 18-kW Cu rotating anode source, Rigaku Corporation, Tokyo, Japan). The surface morphology was studied by ESEM (Philips model XL30, FEI/Philips, Hillsboro, OR). The surface roughness was measured by a surface profilometer (Tencor model P-10, Tencor Inc., San Jose, CA). The solubilities of the coatings were assessed by immersing one sample from each type in 20 mL of distilled water at room temperature (nominally 25 °C). At various immersion periods of one, 24, 48, 72, 216 and 240 h, 1 mL of solution was removed and replaced by 1 mL of fresh distilled water. The volume removed was further diluted to 10 mL by distilled water, and the calcium concentration was measured by a direct current plasma atomic emission spectrometer (DCP-AES, SpectraSpan model III A, Applied Research Laboratories Inc., Valencia, CA).

2.2. Surgery

Samples were implanted into canine trabecular bone for three different periods, as follows, before sacrificing the animal for further analysis: 6 h, 7 and 14 days, respectively. For each period, seven PSHA-coated samples, seven EDHA-coated samples, and six Ti–6Al–4V bare samples were available for TEM/ESEM studies, thus summing to a total of 60 implant samples.

Animal protocols followed were those specifically approved by the institutional animal care and use committee (IACUC) of the Veterans Administration (VA) Hospital in Boston. All samples were implanted in the proximal and distal femora and proximal tibiae of the back legs of adult mongrel dogs, each weighing about 30 kg. A pilot study established that the cancellous bone at these three implant sites was of comparable density. Therefore, the data were not stratified on the basis of implant site or by animal [18].

2.3. ESEM

After sacrifice, tissues intended for ESEM examination were placed in 0.1 M sodium cacodylate-buffered 4% paraformaldehyde and 2% glutaraldehyde solution. Tissue around the rods was trimmed to about 1–2 mm thick. The trimmed samples were fixed in the same buffered solution for 24 h under partial vacuum at 4 °C. Next, the samples were washed in 0.1 M sodium cacodylate buffer solution twice for 10 min in order to remove the fixatives, then stored overnight in the same solution at 4 °C. The samples were subsequently fixed in 1% osmium tetroxide aqueous solution at 4 °C for 2 h. After rinsing in de-ionized water, the samples were dehydrated through a series of 50%, 75%, 95% and 100% ethanol aqueous solutions for 15 min each and then a final 15 min in 100% ethanol. The samples were agitated in 1:3, 1:2, 1:1 and 2:1 Spurr's resin (Ted Pella Inc., Redding, CA) dissolved in ethanol for 24 h each and then vacuum-infiltrated with pure Spurr's resin for 24 h. They were then embedded in fresh Spurr's resin for 24 h at 60 °C. The embedded samples were cut into 0.5 mm-thick slices with a slow-speed diamond saw. All slices were ground on 1200-grit SiC

paper, then polished using 5-μm alumina paste followed by 0.06-μm colloidal alumina in water. The polished specimens were subsequently coated with a thin layer (about 10 nm) of evaporated carbon and observed by ESEM, using the standard ESEM imaging detector.

Micrographs were recorded around the periphery of each implant at magnifications about 100×. For each implant, approximately 20 such images were collected and stored in digital format (1424 × 968 bytes). The lineal surface apposition ratio was calculated following the protocol established in earlier MIT work [18]. The apposition ratio for each implant was eventually taken as the average ratio for all interface images of that implant. The area apposition ratio, defined as the areal fraction of the implant surface covered with new bone, was calculated as the square of the one-dimensional apposition ratio, presuming that the new bone formation was isotropic.

2.4. TEM

Preparation of TEM samples followed the same fixation, dehydration, embedding, and sectioning methods used for ESEM samples. After cutting into thin slices, samples were freeze-fractured to remove the titanium alloy rod. After removing the titanium, the samples were re-embedded in BEEM® vials (Ted Pella) filled with Spurr's resin cured for 24 h at 60 °C. The vials were then carefully removed from the cured resin, and the sample tip was trimmed to a 1-mm^2 cross section to expose the coating/bone interface. Thin sections about 60–80 nm thick were cut using an ultramicrotome (RMC model MT-X, Boeckeler Instruments Inc., Tucson, AZ), collected on parlodion-coated grids (Ted Pella), and air-dried. Some samples were stained in 2% uranyl citrate in 50% alcohol-water solution for 2 h, and then in 0.5% lead citrate aqueous solution for 30 min in order to enhance mass-thickness contrast in TEM. The other samples were left unstained for diffraction contrast study. The microtomed samples were viewed in either JEM 2000FX or JEM 2010 TEM instruments (JEOL Inc., Tokyo, Japan). Elemental analysis was performed using an energy-dispersive X-ray spectrometric (XEDS) detector attached to the JEM 2010 TEM instrument.

3. Results

3.1. Coating characterization

Comparison to the standard JCPDS X-ray diffraction file for HA (No. 09-0432) confirmed that both coatings were substantially composed of crystalline HA (Fig. 1). The crystallinity of HA coatings was quantified using JADE software (Rigaku); the non-crystalline content was found to be about 10% for the PSHA and less than 5% for the EDHA coatings (The Bragg peaks from the titanium substrate, stronger for the thinner EDHA coatings but also present in both patterns, were subtracted prior to analysis). ESEM micrographs established that the thickness of the EDHA coating was about 5 μm, and the PSHA coating about 50 μm.

The surface morphologies of these two coatings were quite different, as shown in Fig. 2a and b, respectively. The EDHA coating was characterized by individually resolvable HA crystallites with a plate-like shape growing normal to the substrate surface. Their typical width was several micrometers and their thickness less than 1 μm, similar to crystals found in HA chemically deposited at room temperature [19]. The surface of PSHA exhibited a dramatically different morphology: large globules appeared at the surface, and no individual HA crystallites could be distinguished; this finding is consistent with molten splats solidifying as individual units with at least partly (probably poly) crystalline character. The size of the surface globules ranged from several micrometers down to about 100 nm. The surface roughnesses (R_a), measured by surface profilometry, were 480 ± 120 nm for EDHA and 1300 ± 400 nm for PSHA coatings, comparing to 465 ± 173 nm for the as-received Ti–6Al–4V rod.

3.2. ESEM measurements of bone apposition ratio

For all three types of implants, both trabecular bone and its debris from the surgery were observed to be present around the implants 6 h after implantation (Fig. 3a–c). Owing to the press-fit method of insertion of the surgical implant, direct contact between bone and implants was also, but infrequently, observed. The shortest implantation time, 6 h, was far too short for a meaningful calculation of new bone apposition ratio for any implant and hence none was calculated.

Seven days after implantation, new bone tissue was observed apposing all three types of implants. The newly developed bone tissue was different from trabecular bone, or its drillhole debris, in that the new tissue closely contacted the implants and spread out over the implant surface. Cellular lacunae were clearly visible in the new bone tissue (Fig. 4a–c).

After 14 days, the surface apposition of new bone tissue had increased on all three types of implants (Fig. 5a–c). At the same time, the new bone tissue became much thicker, denser and more closely conformed to the coating surface topography, especially apparent for PSHA-coated and EDHA-coated implants.

The average surface bone apposition ratios (Fig. 6) for each type of sample after 7 and 14 days implantation were calculated from the ESEM images. Two-factor analysis of variance (ANOVA) revealed that there were significant effects of time ($p < 0.0001$; power = 1) and coating type ($p = 0.0002$; power = 0.99) on the apposition of bone to the samples. Post-hoc testing using Fisher's protected least-squares differences (PLSD) method showed that the difference between the PSHA and Ti–6Al–4V groups was statistically significant ($p < 0.0001$), as was the difference between the EDHA and Ti–6Al–4V groups ($p = 0.002$). There was, however, no statistically significant difference between the PSHA and EDHA groups when including all data from the 7- and 14-day time periods. One-factor ANOVA of the 7-day data also demonstrated that there was a significant effect of the group on the percentage of bone apposed to the surface ($p = 0.16$; power = 0.83). In this case, analyzing the 7-day data separately, there was a statistically significant difference in the apposition to the PSHA and Ti–6Al–4V groups ($p = 0.006$), but there was no statistically significant difference between the PSHA and EDHA groups, and between the EDHA and Ti–6Al–4V groups.

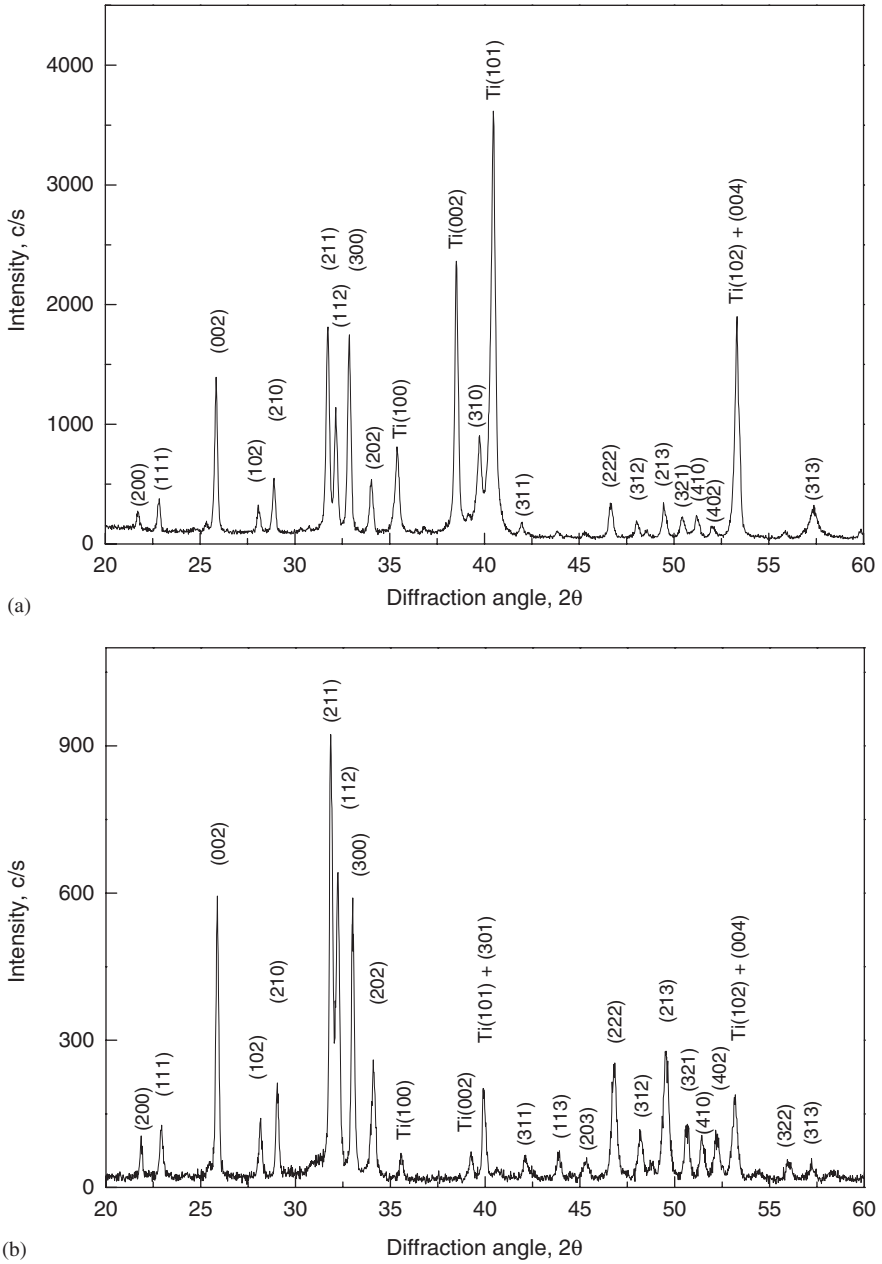

Fig. 1. X-ray diffraction spectra for: (a) EDHA, and (b) PSHA coatings (Cu Kα radiation).

3.3. TEM analysis of the bone/coating interface

TEM study was limited to implants coated with the two forms of HA coatings only because the TEM sample preparation procedure used in this study was not suited to preserving new bone apposing bare Ti–6Al–4V.

In the case of PSHA-coated samples implanted for 6 h (Fig. 7a), bone debris and blood cells were found near the coating surface, but no evidence of mineralized tissue; trabecular bone tissue (from debris or the original bone) was observed only much farther away (not shown in Fig. 7a). The Ca/P atom ratio for the coating, measured by XEDS, was 1.67, matching the stoichiometric value for HA. The image showed an undulating surface on the coating, with possible indications of intergranular dissolution. Small (<100 nm) HA crystalline platelets, likely reprecipitating from dissolved HA coating [18], were sometimes found present within 1 μm of the HA coating surface.

For EDHA-coated samples, 6 h after implantation, the substrate side of the coating was smooth, suggesting that the whole coating had separated from the titanium substrate due to poor bonding between the EDHA and the substrate (Fig. 7b). The edges and corners of the coating crystals opposing the drilled bone remained sharp, with little apparent sign of dissolution. XEDS analysis yielded a Ca/P atom ratio of 1.6, close to that of stoichiometric HA.

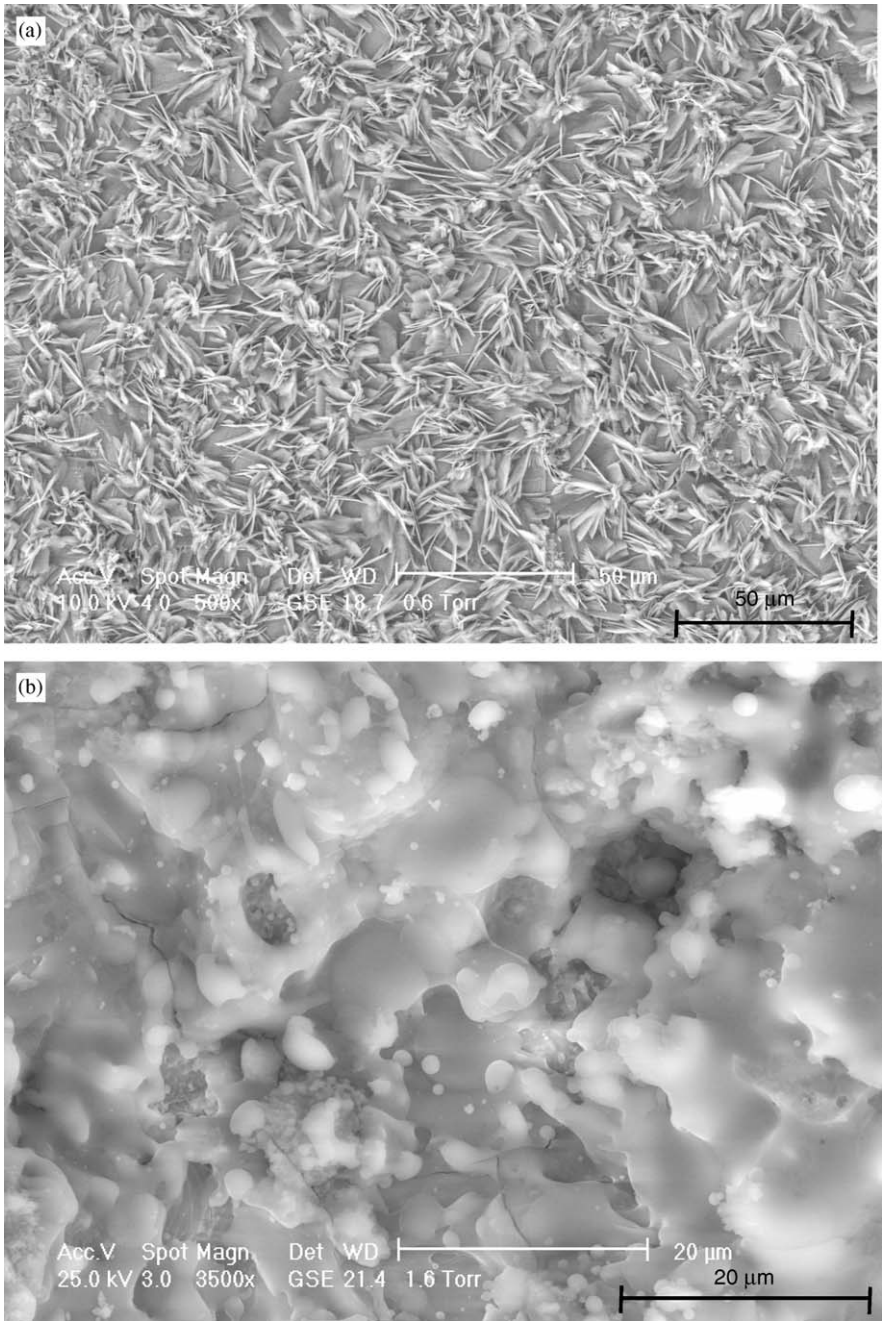

Fig. 2. ESEM images of the two coatings: (a) EDHA surface top view, and (b) PSHA surface top view.

After 7 days implantation, TEM analysis revealed a layer of dense mineralized tissue formed immediately adjacent to the PSHA coating surface (Fig. 8a) and isolated fibrillar mineralized "clusters" further away from the coating interface. Higher resolution images (Fig. 8b and c) of these clusters and the dense layer near the interface showed that they were composed of many fine nano-ribbons, which were several hundred nano-meters long but only several nano-meters wide. Surrounding these clusters was an unmineralized collagenous matrix, whose fibers exhibited the characteristic banded structure visible after lead citrate and uranyl acetate staining. Differently oriented collagen fibers were observed; however, their size was uniform, with diameters consistently less than 50 nm and lengths as long as 1 μm. Collagen fibers were not, however, found within the clusters. XEDS analysis showed that the Ca/P atomic ratio of the clusters was about 1.2, much lower than that of HA but closer to the typical values for brushite (dicalcium phosphate dehydrate, DCPD, $Ca/P = 1.0$), octacalcium phosphate (OCP, $Ca/P = 1.33$), or even amorphous calcium phosphate (ACP, $Ca/P = 1.5$). By comparison, the Ca/P ratio of the HA coating was measured at about 1.6, and that of mature bone tissue also close to 1.6. The surrounding collagen matrix remained largely

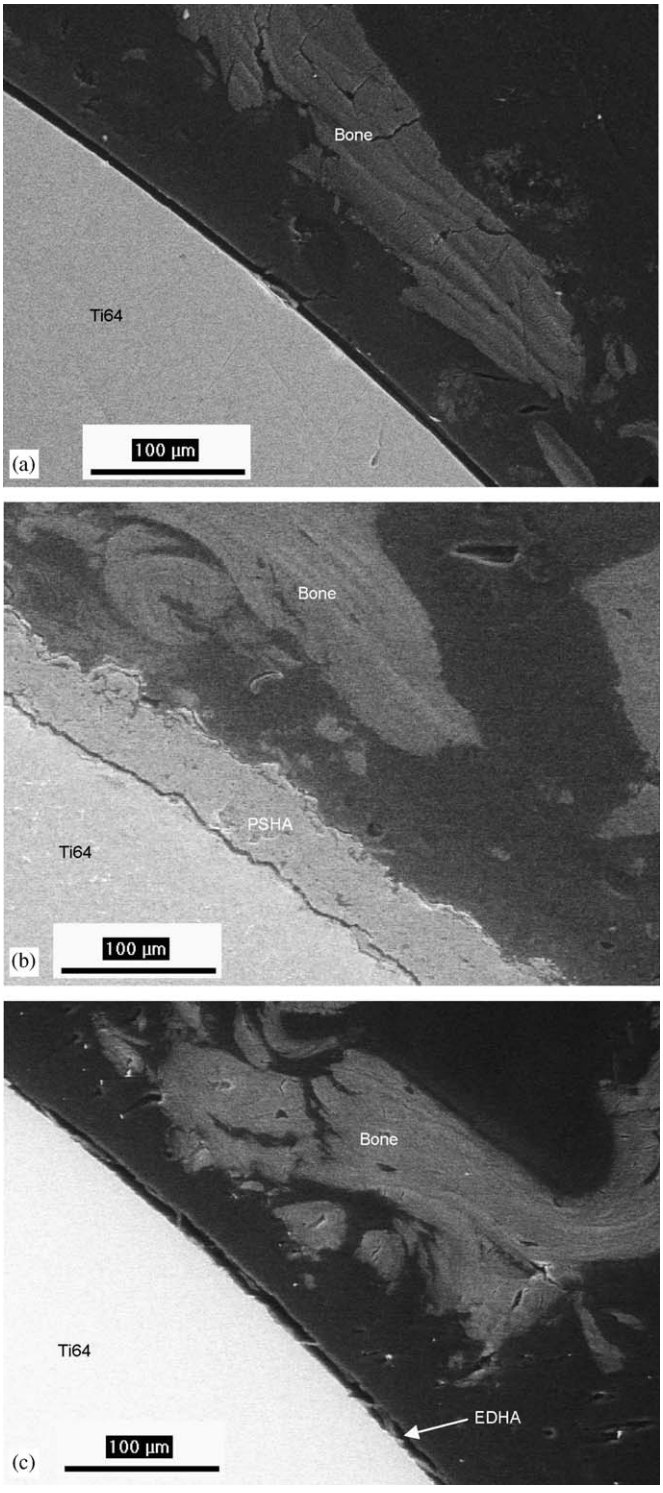

Fig. 3. ESEM images from cross-sections through implants and adjacent bone tissue, 6 h implantation: (a) Ti–6Al–4V, (b) PSHA coating, and (c) EDHA coating.

unmineralized at 7 days, the calcium content remaining very low (less than 1 at%) and phosphorus almost undetectable.

By contrast, little tissue development was seen near the EDHA coating surface 7 days after implantation. Osteoblast-like cells were found in some regions, stationed close to the coating surface, at a distance of approximately 10–15 μm (Fig. 8d). The surface of the coating 1 week after implantation was still similar to that 6 h after implantation.

By 14 days post-implantation, the mineralized tissue layer on the PSHA coating had became much thicker and covered almost the entire surface (Fig. 9a). The characteristic banded structure of stained collagen could be seen in the new bone tissue layer. The Ca/P atom ratio of this tissue increased to nearly 1.7.

Compared to PSHA, new mineralized tissue formation on the EDHA coating increased much more substantially between 7 and 14 days (Fig. 9b). Much new tissue was found on the EDHA surface and closely integrated with the coating, interdigitating with the blade-like EDHA crystals. The Ca/P atomic ratio of the new tissue was close to 1.7. This dramatic increase in proximate mineralized tissue formation matches the increase in bone apposition ratio previously documented in the ESEM observations.

4. Discussion

Both EDHA and PSHA coatings used in this study were composed predominantly of HA and had very close nominal compositions. However, they were distinct in surface topographies, coating morphologies, microstructures, and degree of crystallinity, one or all of which are likely to have resulted in differing solubilities, i.e. their ability to initially release calcium and phosphorus into the environment. A confirmatory solubility test (Fig. 10) showed that PSHA dissolved much more readily than EDHA. While the former reached saturation in distilled water in 2 days, the latter occasioned a very low Ca concentration even after 10 days. It is presumed that the difference in their solubilities is at least partially responsible for the different observed kinetics for early bone formation associated with these two coatings; and it can certainly be stated that the solubility correlates with different onset times for collagen release and its mineralization.

EDHA showed a low bone apposition ratio after 7 days, intermediate between the corresponding values for bare Ti–6Al–4V alloy and PSHA-coated samples. However, after 14 days, the EDHA bone apposition ratio increased markedly, to that observed for PSHA, and much more than that for bare Ti–6Al–4V. The initial low apposition ratio may be attributable to the low solubility of EDHA. During the first 7 days, the coating made almost no contribution to bone apposition via ion release and reprecipitation or by Ca signaling to osteoblasts [20,21]; thus it exhibited almost the same apposition ratio as bare Ti–6Al–4V. PSHA, with its partial amorphous content and consequently higher solubility in vivo, contributed a much higher local concentration of calcium and phosphorus ions, which could assist in and accelerate local mineralization of new bone or be involved in cell signaling. Nevertheless, the differing solubilities dictated only different short-term

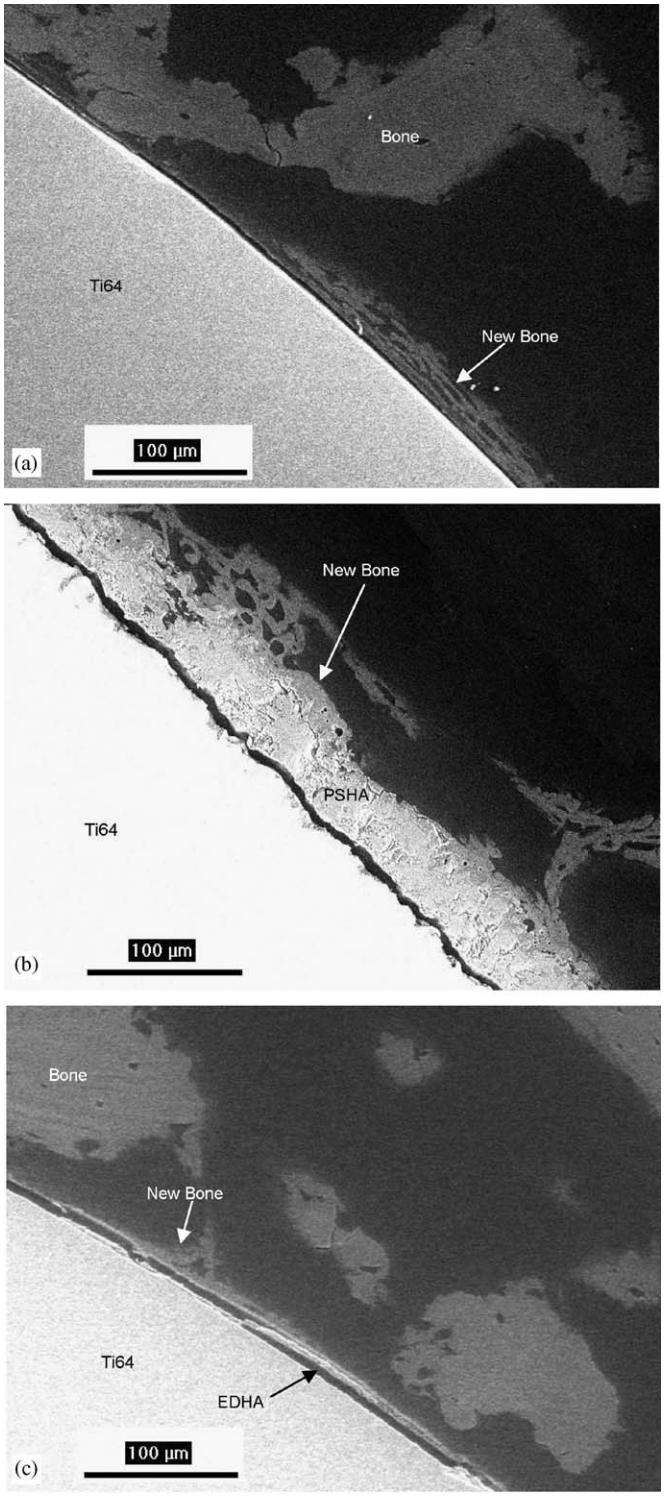

Fig. 4. ESEM images from cross-sections through implants and adjacent bone tissue, 7 days implantation: (a) Ti–6Al–4V, (b) PSHA coating, and (c) EDHA coating.

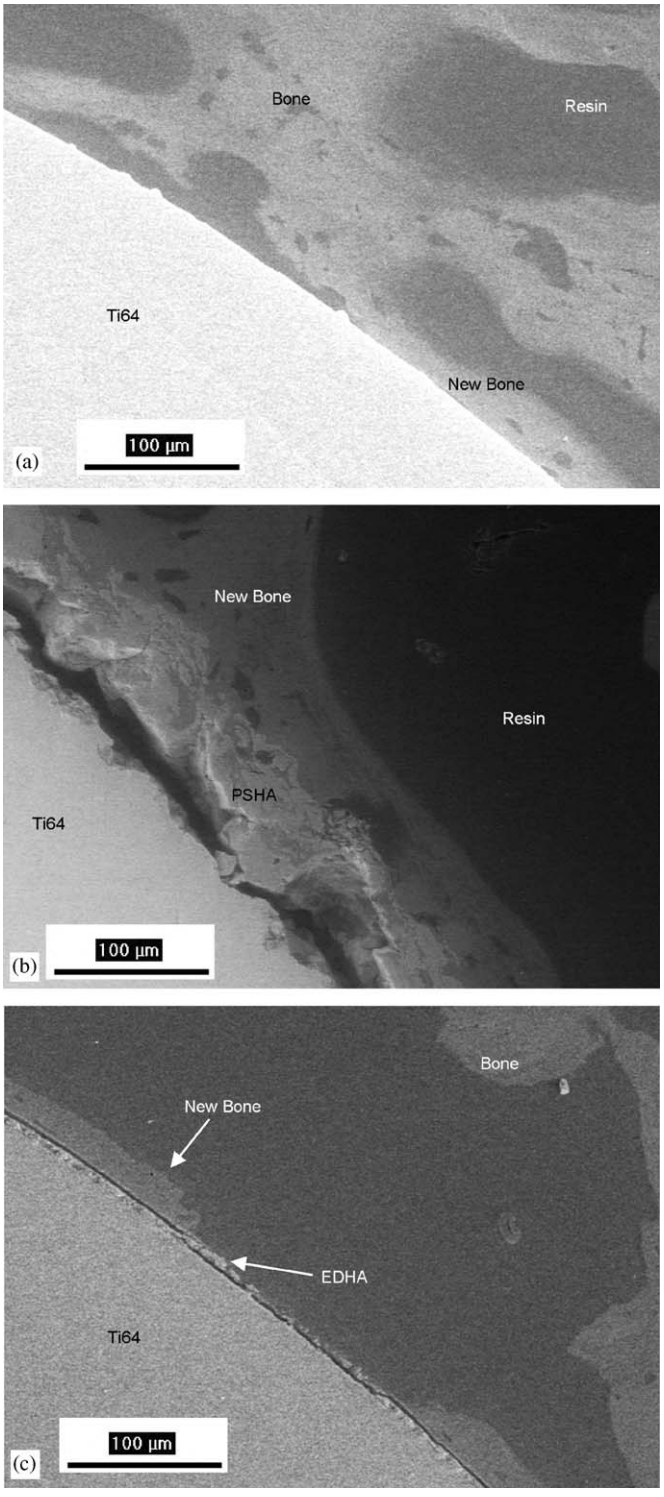

Fig. 5. ESEM images from cross-sections through implants and adjacent bone tissue, 14 days implantation: (a) Ti–6Al–4V, (b) PSHA coating, and (c) EDHA coating.

mineralization behaviors. By 14 days, the surface apposition ratio of EDHA increased sharply and caught up with that of PSHA, suggesting that the lower dissolution rate of EDHA was already sufficient to catalyze the formation of new bone. A similar initial disparity and later catch-up has been reported for annealed vs. non-annealed PSHA coatings [18].

At 7 days post-implantation, new mineralized tissue—mainly composed of clustered nano-ribbons—was observed on the PSHA coatings only. Collagen fibers, visible

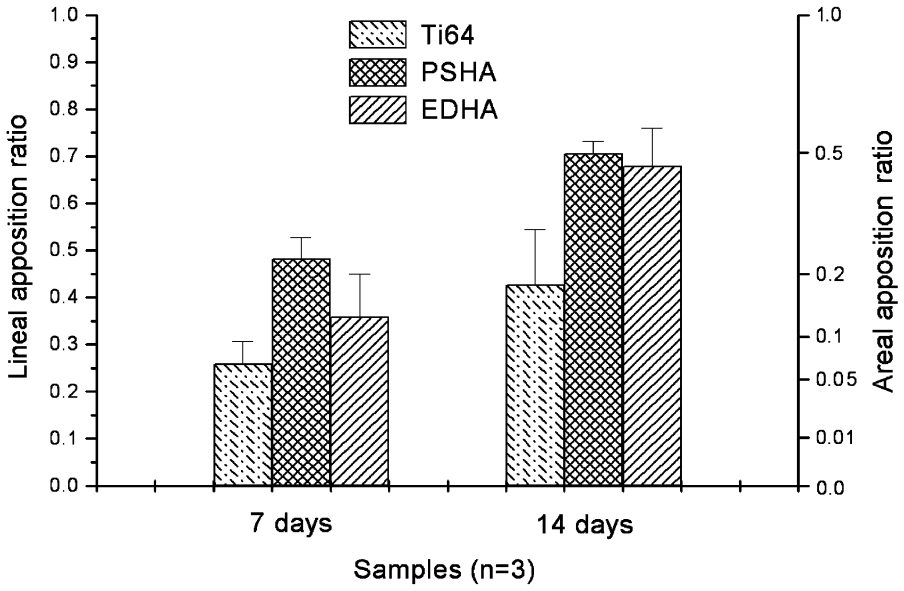

Fig. 6. Average bone apposition ratios after 7 and 14 days of implantation. The error bars are standard deviations.

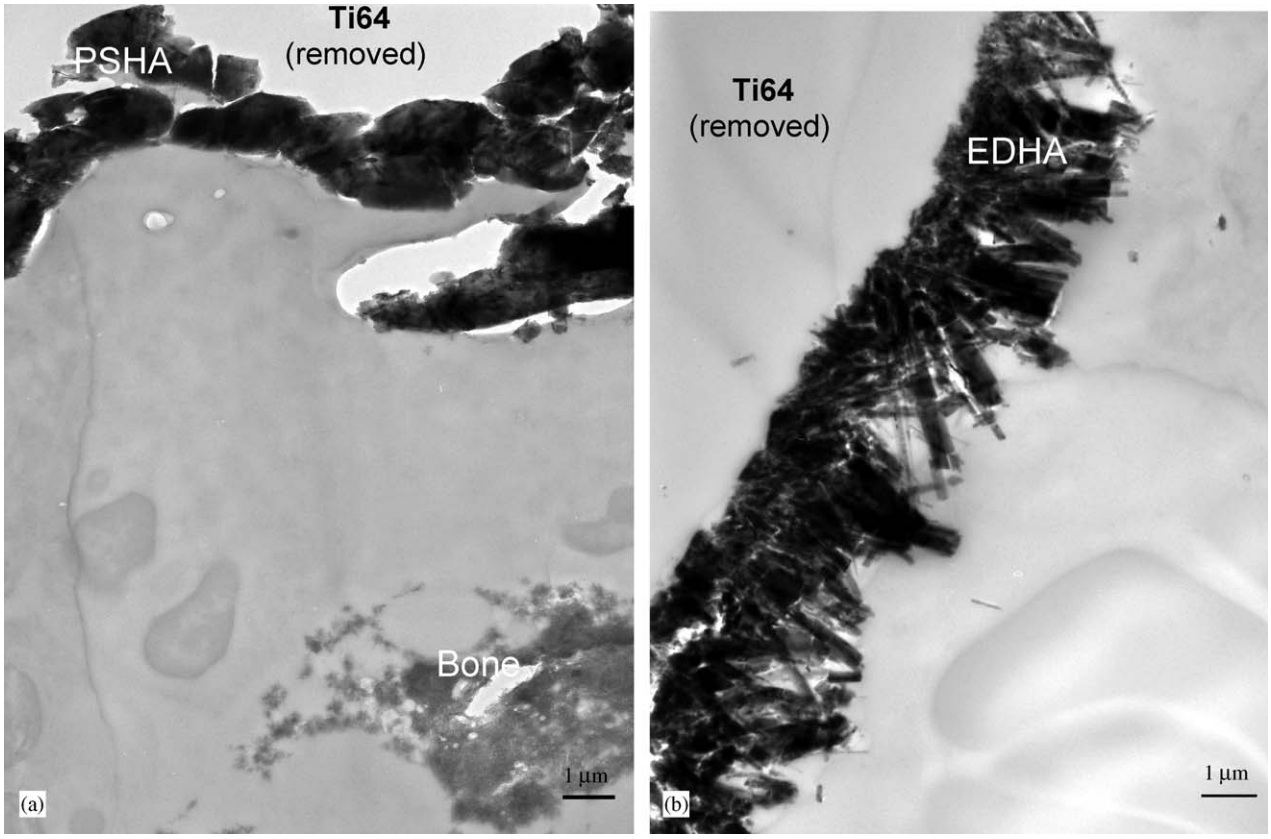

Fig. 7. Cross-section TEM micrographs of samples implanted for 6 h: (a) PSHA, and (b) EDHA. Thin sections were stained with uranyl acetate and lead citrate.

upon staining, were also present close to the coating surface, but were not yet mineralized. After 14 days, new bone-like tissue was already very well developed in the vicinity of both types of coatings, incorporating collagen fibers. Many proteins, among them osteonectin [22], osteocalcin [23] and bone sialoprotein [24], have been hypothesized to serve as nuclei or templates for initial deposition of HA [25]. However, in this study the earliest mineral deposits observed were actually long nano-ribbons, of large aspect ratio, considerably different in morphology

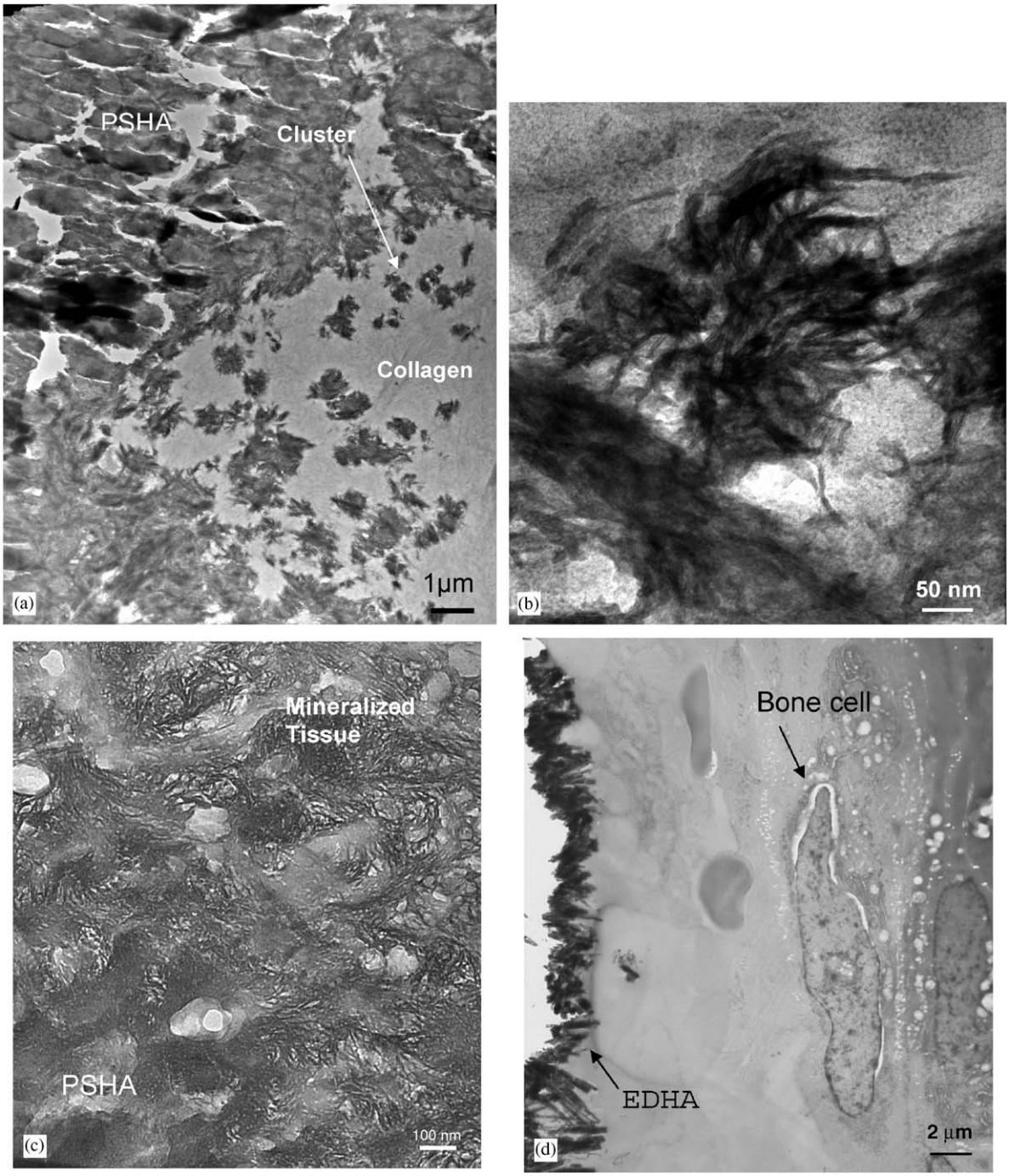

Fig. 8. Cross-section TEM micrographs of samples implanted for 7 days: (a) PSHA coating and mineralized clusters, (b) a detailed image of a mineralized cluster close to PSHA coating surface, (c) detail of newly mineralized tissue at the interface with PSHA coating, and (d) EDHA coating. Cracks were introduced by microtoming PSHA coatings. Thin sections were stained with uranyl acetate and lead citrate.

from the proteins cited. The clustered nano-ribbons were only about several nano-meters in width, but several hundred nm in length. Thus, the potential role of short connective proteins is relegated to nucleation and not templating. The nano-ribbons are, however, very close in size to a single collagen molecule (1.5 nm diameter, 300 nm long) or five-stranded fibrils (about 4 nm diameter) [26]. It has been generally believed that individual collagen molecules do not by themselves have the ability to initiate mineral deposition [27]; however, minimally self-assembled protofibrils (such as the five-strand fiber mentioned above) have been suggested to have the ability to nucleate mineral precipitation along the fibril length on the evidence of a recent in vitro study [28]. Hence, the clustered mineral nano-ribbons could represent calcium phosphates nucleating on individual collagen molecules or minimally stranded

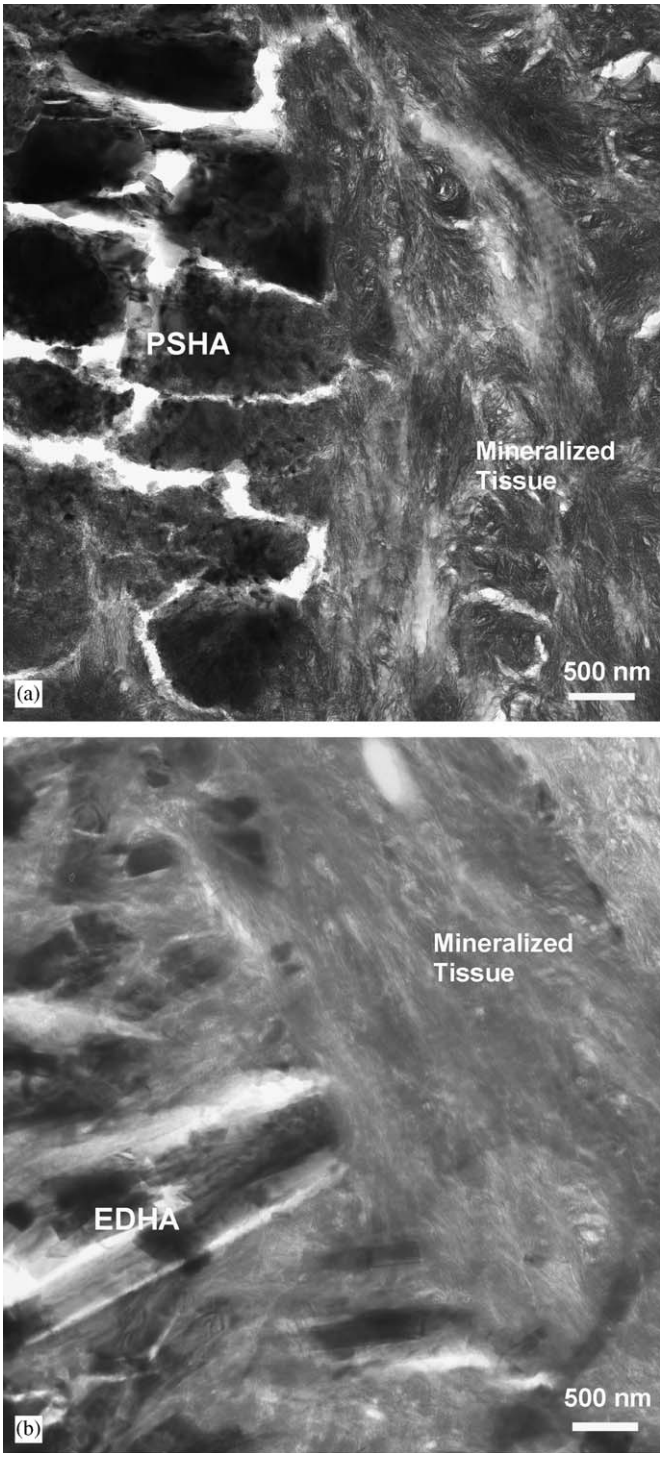

Fig. 9. Cross-section TEM micrographs of samples implanted for 14 day: (a) PSHA, and (b) EDHA coatings. Thin sections were stained with uranyl acetate and lead citrate.

fibrils. This explanation has not been advanced before and remains speculative, pending identification of the nucleating agent. On the other hand, self-assembled collagen fibers in bone are not mineralized along their length, but instead at inter-molecule junctions by crystallographically and morphologically oriented platelets [29] that bear no relationship to collagen molecule length or morphology (except for the molecular self-assembly motif).

A significant observation is the low Ca/P atomic ratio in the early stage mineral nano-ribbon deposits. The value strongly suggests that HA is not the initial calcium phosphate phase involved in the earliest stage of mineralization. It has been observed in vitro that ACP and OCP, which have more favorable formation kinetics than HA, are deposited before HA on NaOH-treated titanium surfaces [30]. The present study has shown that the same may occur for bone formation in vivo. Theories of protein control of bone mineralization have mainly focused on the shape and size match between proteins and the HA unit cell [31,32]. However, the present observations suggest that the role of proteins in nucleating calcium phosphates of other stoichiometries, such as ACP, DCPD, and OCP, could be initially more important.

EDHA, as a potential substitute for PSHA, confers some advantages, such as low processing temperature and deposition on complicated shapes. The platey surface morphology of EDHA coatings may be particularly efficacious in promoting integration of newly mineralized tissue with the HA coating and in maximizing the mechanical integrity of the coating-bone interface, However, low bonding strength between coating and substrate was also observed. This drawback could be overcome by tailoring the substrate composition or topography before electrodeposition—for example, by mechanically or chemically texturing the substrate surface or by pre-forming a hydrogel surface layer [33] onto Ti alloy surfaces. Though the EDHA coatings were substantially thinner than the PSHA coatings, it has been shown [34] that even thick (50 μm) PSHA coatings appear to be substantially remodeled eventually, after months or years of implantation in human models. The much thinner EDHA coatings can nevertheless still prove efficacious over the critical weeks-to-months period for establishment of apposing mineralized tissue, before substantial remodeling has occurred; and when substantial remodeling does begin, the initial coating thickness may be irrelevant.

5. Conclusions

In agreement with a previous in vivo study [18], PSHA coatings of implantation into canine trabecular bone were found to accelerate early stage mineralization of bone tissue formation over that occurring for bare alloy implants. Kinetic differences in the early stage ($\leqslant$7 days) of observed mineralization correlated closely to differences in coating solubilities, though later-stage (14 days) mineralization rates were relatively unaffected. The early stage mineral product had a morphology (nano-ribbon clusters) and composition (Ca/P$\sim$1.2) distinguishably different from that of mature bone, likely representing a calcium phosphate phase with lower Ca/P ratio (DCPD, ACP, OCP). Though smaller proteins may direct the peculiar

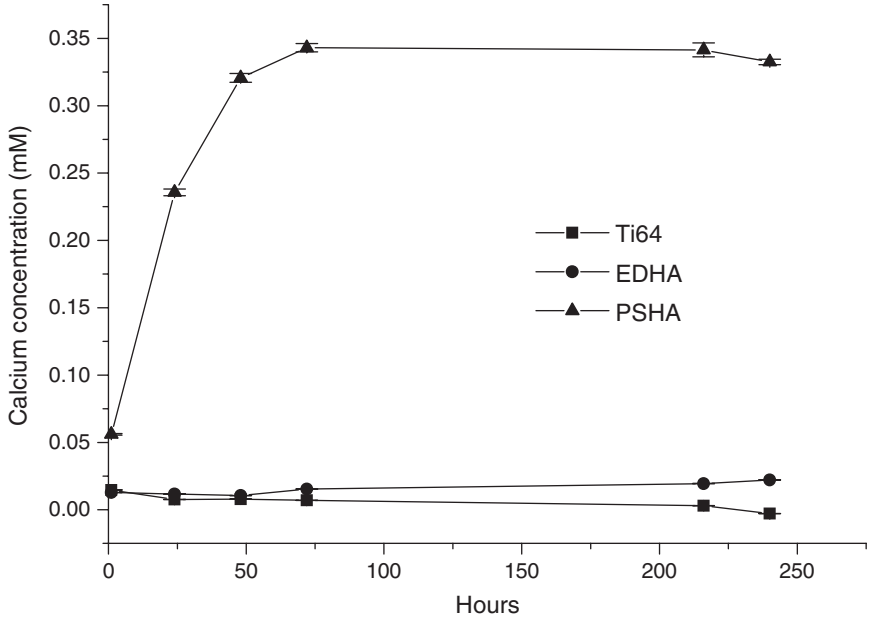

Fig. 10. Aqueous solubilities of PSHA and EDHA in de-ionized water at room temperature. Bare Ti–6Al–4V alloy serves as a reference ($n = 1$; error bars are standard deviations from three measurements).

nano-ribbon growth morphology, mineralization could be occurring along the length of single collagen molecules or minimally stranded collagen fibrils. EDHA coatings were slower in inducing early stage mineralization ($\leqslant 7$ days) than PSHA coatings but were more efficacious than bare Ti–6Al–4V alloy, and were indistinguishable from PSHA coatings in the later (14 days) mineralized tissue apposition ratio and microstructure they induced in vivo. The surface morphology and higher surface area of EDHA coatings appear to have resulted in better mechanical integration of coating and mineralized tissue. The low adhesion of EDHA coatings to substrates will need to be addressed to better realize the promise inherent in electrodeposition coating approaches.

Acknowledgments

This work was supported by the Division of Bioengineering and Environmental Systems of the US National Science Foundation under award DMR-9904046, the Cambridge-MIT Institute, and the John F. Elliott chair (LWH). The authors are grateful to Dr. T.M. Sridhar for preparing the EDHA coatings. The VA Boston Healthcare System provided the facility for animal surgeries at their Jamaica Plain campus.

References

[1] Overgaard S. Calcium phosphate coating for fixation of bone implants. Acta Orthop Scand 2000;71:1–74.
[2] Soballe K, Hansen ES, Rasmussen HB, Jorgensen PH, Bunger C. Tissue ingrowth into titanium and hydroxyapatite-coated implants during stable and unstable mechanical conditions. J Orthop Res 1992;10:285–99.
[3] Thomas KA, Cook SD, Haddad Jr RJ, Kay JF, Jarcho M. Biologic response to hydroxylapatite-coated titanium hips. A preliminary study in dogs. J Arthroplasty 1989;4:43–53.
[4] Wen HB, de Wijn JR, Cui FZ, de Groot K. Preparation of calcium phosphate coatings on titanium implant materials by simple chemistry. J Biomed Mater Res 1998;41:227–36.
[5] Suchanek W, Yoshimura M. Processing and properties of hydroxyapatite-based biomaterials for use as hard tissue replacement implants. J Mater Res 1998;13:94–117.
[6] Luo ZS, Cui FZ, Li WZ. Low-temperature crystallization of calcium phosphate coatings synthesized by ion-beam-assisted deposition. J Biomed Mater Res 1999;46:80–6.
[7] Spoto G, Ciliberto E, Allen GC. A new synthetic route to hydroxyapatite coatings. J Mater Chem 1994;4:1849–50.
[8] Russell SW, Luptak KA, Suchicital CTA, Alford TL, Pizziconi VB. Chemical and structural evolution of sol–gel-derived hydroxyapatite thin films under rapid thermal processing. J Am Ceram Soc 1996;79:837–42.
[9] Tucker BE, Cottell CM, Auyeung RC, Spector M, Nancollas GH. Pre-conditioning and dual constant composition dissolution kinetics of pulsed laser deposited hydroxyapatite thin films on silicon substrates. Biomaterials 1996;17:631–7.
[10] Ducheyne P, Radin S, Heughebaert M, Heughebaert JC. Calcium-phosphate ceramic coatings on porous titanium—effect of structure and composition on electrophoretic deposition, vacuum sintering and in vitro dissolution. Biomaterials 1990;11:244–54.
[11] Shirkhanzadeh M. Calcium-phosphate coatings prepared by electrocrystallization from aqueous-electrolytes. J Mater Sci-Mater Med 1995;6:90–3.
[12] Shirkhanzadeh M. Bioactive calcium-phosphate coatings prepared by electrodeposition. J Mater Sci Lett 1991;10:1415–7.
[13] Redepenning J, McIsaac JP. Electrocrystallization of brushite coatings on prosthetic alloys. Chem Mater 1990;2:625–7.
[14] Shirkhanzadeh M. Electrochemical preparation of bioactive calcium-phosphate coatings on porous substrates by the periodic pulse technique. J Mater Sci Lett 1993;12:16–9.

[15] Shirkhanzadeh M. Direct formation of nanophase hydroxyapatite on cathodically polarized electrodes. J Mater Sci-Mater Med 1998;9:67–72.
[16] Vijayaraghavan TV, Bensalem A. Electrodeposition of apatite coating on pure titanium and titanium-alloys. J Mater Sci Lett 1994;13:1782–5.
[17] Royer P, Rey C. Calcium-phosphate coatings for orthopedic prosthesis. Surf Coat Technol 1991;45:171–7.
[18] Porter AE, Hobbs LW, Rosen VB, Spector M. The ultrastructure of the plasma-sprayed hydroxyapatite-bone interface predisposing to bone bonding. Biomaterials 2002;23:725–33.
[19] Feng QL, Wang H, Cui FZ, Kim TN. Controlled crystal growth of calcium phosphate on titanium surface by NaOH-treatment. J Cryst Growth 1999;200:550–7.
[20] Tfelt-Hansen J, Brown EM. The calcium-sensing receptor in normal physiology and pathophysiology: a review. Crit Rev Clin Lab Sci 2005;42:35–70.
[21] Hofer AM. Another dimension to calcium signaling: a look at extracellular calcium. J Cell Sci 2005;118:855–62.
[22] Termine JD, Kleinman HK, Whitson SW, Conn KM, McGarvey ML, Martin GR. Osteonectin, a bone-specific protein linking mineral to collagen. Cell 1981;26:99–105.
[23] Hauschka PV, Lian JB, Gallop PM. Direct identification of calcium-binding amino-acid, gamma-carboxyglutamate, in mineralized tissue. P Natl Acad Sci USA 1975;72:3925–9.
[24] Oldberg A, Franzen A, Heinegard D. The primary structure of a cell-binding bone sialoprotein. J Biol Chem 1988;263:19430–2.
[25] Hunter GK, Hauschka PV, Poole AR, Rosenberg LC, Goldberg HA. Nucleation and inhibition of hydroxyapatite formation by mineralized tissue proteins. Biochem J 1996;317:59–64.
[26] Smith JW. Molecular pattern in native collagen. Nature 1968;219:157–8.
[27] Veis A. Mineralization in organic matrix frameworks. Rev Mineral Geochem 2003;54:249–89.
[28] Zhang W, Liao SS, Cui FZ. Hierarchical self-assembly of nano-fibrils in mineralized collagen. Chem Mater 2003;15:3221–6.
[29] Rosen VB, Hobbs LW, Spector M. The ultrastructure of anorganic bovine bone and selected synthetic hydroxyapatites used as bone graft substitute materials. Biomaterials 2002;23:921–8.
[30] Feng QL, Cui FZ, Wang H, Kim TN, Kim JO. Influence of solution conditions on deposition of calcium phosphate on titanium by NaOH-treatment. J Cryst Growth 2000;210:735–40.
[31] Hoang QQ, Sicheri F, Howard AJ, Yang DS. Bone recognition mechanism of porcine osteocalcin from crystal structure. Nature 2003;425:977–80.
[32] Sarig S. Aspartic acid nucleates the apatite crystallites of bone: a hypothesis. Bone 2004;35:108–13.
[33] Wen HB, de Wijn JR, Cui FZ, de Groot K. Preparation of bioactive Ti6Al4 V surfaces by a simple method. Biomaterials 1998;19:215–21.
[34] Porter AE, Taak P, Hobbs LW, Coathup MJ, Blunn GW, Spector M. Bone bonding to hydroxyapatite and titanium surfaces on femoral stems retrieved from human subjects at autopsy. Biomaterials 2004;25:5199–208.